HHS Public Access

Author manuscript

Nano Energy. Author manuscript; available in PMC 2020 September 17.

Published in final edited form as:

Nano Energy. 2019 June ; 60: 17–25. doi:10.1016/j.nanoen.2019.03.032.

All printable snow-based triboelectric nanogenerator

Abdelsalam Ahmed[a,b,c,*], **Islam Hassan**[b], **Islam M. Mosa**[d,e], **Esraa Elsanadidy**[d], **Gayatri S. Phadke**[d], **Maher F. El-Kady**[f,g], **James F. Rusling**[d,h,i], **Ponnambalam Ravi Selvaganapathy**[b,c], **Richard B. Kaner**[e,f]

[a]School of Mechanical & Industrial Engineering, University of Toronto, Toronto, ON, M5S 3G8, Canada [b]Department of Mechanical Engineering, McMaster University, Hamilton, ON, L8S 4L7, Canada [c]Department of Biomedical Engineering, McMaster University, Hamilton, ON, L8S 4L7, Canada [d]Department of Chemistry, University of Connecticut, Storrs, CT, 06269, United States [e]Department of Chemistry, Tanta University, Tanta, Egypt, 31527 [f]Department of Chemistry and Biochemistry and California NanoSystems Institute, University of California, Los Angeles (UCLA), Los Angeles, CA, 90095, United States [g]Department of Materials Science and Engineering, UCLA, Los Angeles, CA 90095, United States [h]Department of Surgery and Neag Cancer Center, UConn Health, Farmington, CT, 06032, USA [i]School of Chemistry, National University of Ireland, Galway, H91 TK33, Ireland

Abstract

The development of power generators that can function in harsh snowy environments and in contact with snow can be beneficial but challenging to accomplish. Herein, we introduce the first snow-based triboelectric nanogenerator (snow-TENG) that can be used as an energy harvester and a multifunctional sensor based on the principle of snow-triboelectrification. In this work, we used a 3D printing technique for the precise design and deposition of the electrode and triboelectric layer, leading to flexible, stretchable and metal-free triboelectric generators. Based on the single electrode mode, the device can generate an instantaneous output power density as high as 0.2 mW/m^2, an open circuit voltage up to 8 V, and a current density of 40 $\mu A/m^2$. In addition, the snow-TENG can function as a miniaturized weather station to monitor the weather in real time to provide accurate information about the snowfall rate, snow accumulation depth, wind direction, and speed in snowy and/or icy environments. In addition, the snow-TENG can be used as a wearable power source and biomechanical sensor to detect human body motions, which may prove useful for snow-related sports. Unlike conventional sensor platforms, our design works without the need for batteries or image processing systems. We envision these devices could potentially be integrated into solar panels to ensure continuous power supply during snowy weather conditions.

Keywords

All printable; Snow-triboelectrification; Arctic; Energy harvesting; Self-powered; Weather station; Wearables

[*]Corresponding author. School of Mechanical & Industrial Engineering, University of Toronto, Toronto, ON, M5S 3G8, Canada. ahmea14@mcmaster.ca (A. Ahmed).

1. Introduction

Access to green, renewable power sources, including solar energy and wind turbines, in areas with frequent snowfall, poses a significant challenge. Severe weather conditions, such as prolonged cloud cover, short daylight periods, heavy snow accumulation, and sub-zero temperatures, can affect energy generation [1,2]. Alternate methods that exploit local weather conditions in these settings could offer a more viable energy generation strategy. Concurrently, continuous meteorological observation is also essential in these cold or snowy environments for all forms of daily activities. However, typical weather stations and meteorological sensors have several limitations, such as their ability to function with snow accumulation, large form factor, cost, complexity and most importantly, the need for a sustainable power source to operate effectively in such severe environments [3,4]. In this scenario, a self-powered multifunctional weather station is a logical choice, but one does not yet exist. This issue is complicated by snow cover that comprises the largest area of the cryosphere, an average of 46 million square kilometers of the Earth's surface each year [5].

The natural phenomenon of snow particles carrying electrical charges (i.e., snow electrification) during snowfall was previously observed, but has remained a curiosity and has not been adequately exploited for useful purposes [6–11]. The snow electrification is based on the ordering of the electric dipoles of water molecules as they crystallize into snowflakes and also can be generated frictionally due to the relative motion between the sliding layer and snow [6,8,11]. The voltage difference generated through the friction of snow with charged surfaces can be affected by several parameters such as the frictional force and surface charge density [6,7,11]. Temperature can also be critical to snow electrification. For instance, it was observed that the snow layer is charged positively at temperatures of −5 °C and −10 °C and negatively at −15 °C and −20 °C [12,13]. Triboelectric Nanogenerators (TENGs) have recently attracted attention as an efficient energy harvesting technology. Various forms of mechanical energy induced by vibration, ocean waves, raindrops, and wind can be converted into electrical energy through the principle of contact electrification [14–26]. Among these, water waves and waterfalls, can be excellent sources of energy with potential for large-scale applications. While there have been many research efforts to extract this water-based energy [19,27–29], none of these efforts has been directed at extracting energy from snow.

Here, we present, for the first time, a snow-triboelectric nanogenerator (snow-TENG) that is designed to harvest energy originating from the contact/friction with snow. The device, operating in a single electrode mode, is designed to utilize both contact electrification and electrostatic induction during a snowfall event. This is made possible by exploiting various kinds of relative motions including snow falling on the surface of the device as well as sliding of snow particles past the device. The snow-TENG output can reach high voltages of up to 8 V with a crest current density of 40 $\mu A/m^2$. Snow-TENG, connected to a load resistor of 50 MΩ, produces an output power density as high as 0.2 mW/m^2. This device functions not only as an energy generator but also as a self-powered multifunctional sensor for various applications. We also demonstrate the potential of this device as an arctic weather station that can measure different meteorological parameters, such as snowfall rate and its direction, wind speed, and depth of snow accumulation. Such a compact and self-

powered sensor could also find applications in performance monitoring for winter sports such as skating and skiing where current unwieldy video analysis equipment are used to assess and improve an athlete's kinematics [30,31]. Furthermore, taking advantage of its lightweight and stretchability, we successfully demonstrate the ability of the snow-TENG as a wearable power source and as a self-powered device for monitoring biomechanical physical activity. Subsequently, we can track various kinds of human activity, such as running, walking, jumping and marching by attaching snow-TENG onto a pair of shoes. Given its low cost, mechanical durability, and ease of fabrication, this wearable snow-based TENG shows potential in a wide range of applications including wearable and environmental sensors and as a sustainable power source in cold climates.

2. Results and discussions

We utilized a 3D extrusion printing approach for fabricating the snow-TENG not only to ensure low-cost and scalable manufacturing but also to allow a high degree of customization in the size and shape of the devices. In this process, the snow-TENG device is constructed by deposition of successive thin films of PEDOT: PSS as an electrode and UV curable silicone as a triboelectrification layer, as illustrated in Fig. 1. The extrusion printing relies on the properties of the inks, which tend to have a considerable influence on the structure and performance of the printed subject. These inks should have high viscosity and shear-thinning behavior to enable controlled flow through nozzles. Considering its flexibility and environmental stability, PEDOT: PSS should be an excellent electrode for transparent snow-TENGs. This conductive polymer is commercially available as a dispersion in water, but lacks reasonable electronic conductivity. The addition of dimethyl sulfate (DMS) ensures higher electronic conductivity of up to 100 S/cm (see methods section). Increased viscosity has been achieved by evaporating extra water. After adjusting its viscosity, this ink is extruded into a thin electrically conductive film on a printed silicone substrate (Fig. 1a–i) and is subsequently thermally cured. Then, a thin film of silicone is printed on the cured electrode layer (Fig. 1a–ii).

Here, pendent thiol propyl silicones are utilized as cross-linkers and telechelic vinyl-substituted silicones as receptors, while TPO-L is added as a photo-initiator in the formulation. This layer can be cured at low temperatures using UV light, leading to mechanically strong, yet flexible and stretchable, silicone-based triboelectric generators. Fig. 1b shows a schematic illustration of the device structure. The surface of silicone has been patterned with an array of microscopic squares/cubes to increase the efficiency of the nanogenerator by increasing the surface area of the contact. SEM analysis of the resulting patterned array shows uniform microstructures with a feature size of 25 μm (see methods section). The device creates electricity through the principle of snow triboelectrification when the falling airborne snow particles come in contact with the silicone surface, as schematically illustrated in Fig. 1c. It is worth noting that the different layers of the device are highly transparent (Fig. 1d). With further developments, this device could be printed directly onto the surface of solar panels to create electricity during snow seasons without compromising the efficiency of the solar cells. It is also interesting to realize that the snow-TENG device is highly stretchable, as demonstrated in Fig. 1e, achieving maximum stretchability of approximately 125%.

To investigate the electrical output of a snow-TENG, a “triboelectric series” of four different triboelectric materials were selected based on their ability to gain or lose electrons and tested in contact with the snow. This includes some materials at the negative scale of the triboelectric series, such as silicone, polytetrafluoroethylene (PTFE), others at the middle section, such as Kapton, and finally, some positive tribomaterials, such as aluminum (Al) [32]. Open circuit voltage $V_{oc,}$ and current density J_{sc} between the snow layer and selected tribomaterials are recorded, as seen in Fig. 2a. Results indicate that V_{oc} and J_{sc} increase steadily depending on the position of the material in the triboelectric series while achieving maximum performance with the most tribo-negative materials. For instance, the contact of snow particles and silicone produced the maximum V_{oc} (8 V), and J_{sc} (24 μA/m^2), whereas snow and Al produced the minimum V_{oc} (1 V), and J_{sc} (2 μA/m^2). Based on the difference in output signals, the snow can be defined as a tribopositive material.

While the selection of the proper triboelectric material is critical, fine-tuning of its surface structure, surface charges, and other physical properties is also necessary for ensuring high-performance TENGs. This was achieved by exploring the effect of curing conditions, such as UV intensity and curing time, on the snow-TENG performance. It was previously discovered that UV light intensity could help in the production of negative charges on the surface of silicone [33]. However, if the UV-exposure time exceeds a specific critical value (6 min as reported), the local charge distribution declines rapidly, and the surface potential in the entire zone slowly achieves a saturation state [34]. It was also reported that UV light irradiation could increase the contact angle of silicone, leading to surfaces with anti-icing properties [35,36]. Therefore, we systematically studied the influence of UV light intensity and curing time on the performance of a snow-TENG. Results in Fig. 2b and c, indicate that the exposure of the silicone layer to a UV light with an intensity of 76 W for 6 min delivers the best performance for the snow-TENG.

The fabricated single electrode snow-TENG can operate through various modes of triboelectrification, such as tapping, sliding and snowfall. In the tapping scenario, as shown in Fig. 3a, the silicone layer does not exhibit a surface charge prior to contact with the snow. Surface groups on the silicone layer will be ionized as the contact event occurs, causing the development of a net negative charge on the silicone surface and a net positive charge on the snow surface (to maintain electrical neutrality). The negative charges remain on the silicone surface as it moves away from the snow, creating a potential difference between the ground and the silicone electrode. Alternatively, the snow-TENG can also generate contact electrification in the sliding scenario, as shown in Fig. 3b. Here too, no charge transfer occurs unless silicone comes in contact with the snow. As silicone slides on the snow, surface groups on the silicone develop negative charges, while electrical neutrality is maintained by the generation of positive charges on the snow surface. The negative charges remain on the surface of silicone as the snow slides off, creating a potential difference between the ground and the silicone layer.

Finally, triboelectric charges can also be generated when snow falls on the silicone thin film, as shown in Fig. 3c. As snow/ice slides on the silicone layer, triboelectricity is produced, resulting in the formation of charged snow particles and a charged silicone surface. When the falling snow comes into contact with the thin film of silicone, the film becomes

negatively charged due to ionization of surface groups. As the snow leaves the silicone layer, a potential difference develops between the ground and the electrode. This potential difference results in an instantaneous negative current flow when the electrode is connected to the ground through a load resistor, as illustrated in Fig. 3c. Further contact with additional snowfall on the surface of the silicone film leads to an increasing amount of electrification and thus, charge density on the surface continues to increase. This increased charge density leads to a corresponding increase in the charges on the electrode that could be measured. This cycle can be repeated as long as snow particles continue to fall, touch, and leave the surface of the snow-TENG device.

A finite element method (FEM) analysis was carried out to show the electrical potential distribution of the snow-TENG in case of three proposed configurations, i.e., tapping, sliding, and snowfall scenarios. The snow-TENG was connected to ground and was assigned a uniform 50 μC cm^2 triboelectric charge density. Using COMSOL software, the charge transfer between the snow-TENG electrode and ground was modulated by changing the relative distance between the snow and the silicone layer in the case of tapping mode or relative lateral distance in the case of sliding mode. At the contact area, the electrical potential approaches zero (Fig. 3d and e). When the two materials are separated, the electrical potential difference increases dramatically, reaching a maximum of 5 V at a distance of 10 mm (in the case of tapping, Fig. 3d) and 10 V at a distance 15 mm (in the case of sliding, Fig. 3e). On the other hand, simulated results for the snow-TENG in snowfall scenarios show an increasing electrical potential difference between the silicone layer and the snow (Fig. 3f). When the snow particle leaves the silicone layer, the electrical potential difference increases dramatically, reaching a maximum of 2 V.

The testing setup for the tapping scenario is presented in Fig. 4a, revealing the snow layer and the TENG attached to a vertical linear motor whereby the release and loading cycles produced consistent electrical output (See supporting video 1). Because of induced capacitance at the contact area, the snow-TENG has relatively good electrical output with matched external resistance. In the tapping scenario, at a frequency of 3 Hz, the snow-TENG registers a V_{oc} of ~6 V and an I_{sc} of 20 μA/m^2 (Fig. 4b and c). The power output of the device depends on the load resistance, with instantaneous power reaching a peak value of approximately 0.06 mW/m^2 at a load resistance of 100 MΩ, Fig. 4d. Fig. 4e shows the charging behavior of a 1 μF capacitor using the output from the snow-TENG. Results show that the capacitor can charge to 2 V in almost 4 min. Interestingly, there is no apparent degradation in voltage profiles for the designed snow-TENG even after about 8000 cycles of repeated loading and unloading at a frequency of 3 Hz, as seen in Fig. 4f. This confirms that snow-TENG is a durable and stable device, even with long-term usage.

Supplementary video related to this article can be found at https://doi.org/10.1016/j.nanoen.2019.03.032.

To demonstrate snow-TENG's capability for scavenging unused friction energy, such as from rolling tires on the snow (Fig. 4g), the device is attached onto a rubber bicycle wheel, and its friction energy scavenging performance was experimentally examined. The experimental setup is shown in Fig. 4h where the snow-TENG has been attached to a bicycle

tire, and the sliding contact between snow and the device during cycling produces an electrical signal that can be harvested. In this sliding mode triboelectric generation, a V_{oc} of ~8 V and an I_{sc} of 40 μA/m^2 (see Fig. 4i and j) were obtained. The power output of the snow-TENG device is higher by almost two times in the sliding scenario than with tapping, with instantaneous power reaching a peak of approximately 0.2 mW/m^2 at a load resistance of 50 MΩ (Fig. 4k).

Given its capability for detecting and harvesting energy from falling snow, the snow-TENG has a huge potential as a self-powered multifunctional cold weather station. This includes measurement of different meteorological parameters, such as snowfall rate and accumulation depth. For example, after adjusting the experimental setup towards the direction of snowfall, we found that the output signal depends on the angle of the falling snow. This is manifested by Fig. 5a, in the snowfall mode, where the snow-TENG can detect snowfall angles of 0°, 45°, and 90° at a constant wind speed of 10.8 km/h and a falling snow rate of 1 cm/min. The increase of the output signal occurs as a larger effective surface area is exposed to the snowfall as the angle increases. For instance, as the device angle increases up to 90° (normal to the direction of the snowfall), the snow impacts a larger surface area of the snow-TENG leading to higher output. In addition, as shown in Fig. 5b and c, the snow-TENG can be used to measure other meteorological parameters such as the snowfall rate as well as the wind speed. While sensing the snowfall rate at a constant angle of 90° and wind speed of 10.8 km/h, the generated electrical signal increases with a higher falling rate as more snow impacts the exposed area of the device. However, measuring the speed of wind depends on the snow impact. The wind increases the impact force of snow particles on the surface of the device, which increases the electrical output as a result (Fig. 5c). It is worth mentioning that all wind speed measurements are recorded at a snowfall rate of 1 cm/min and the device angle of 45°.

Using the sliding mode, as shown in Fig. 5d, a snow-TENG can also measure the depth of snow accumulation when inserted into a snow precipitate on the ground. As the accumulated snow depth increases from 1.0 cm to 3.0 cm, the contact area of snow with the device also increases, and this is reflected in the increase in electric output. The snowfall rate and wind speed data were obtained from the reported values on the weather network on the day of the measurements. All the measurements were conducted outdoors, using the snowfall scenario, under the following conditions: Temperature of −6 °C, humidity of 60%, and snow particle diameters less than 1 cm. Electrical output measurements yield a clear correlation with the measured parameters, indicating the snow-TENG's ability to measure parameters of meteorological significance (Fig. 5a–d). This multi-parametric snow-TENG sensing platform can be developed to measure multiple parameters simultaneously with the help of signal-processing techniques for analyzing the time-domain signal to separate the contribution of each stimulus.

Thanks to its stretchability, lightweight, and conformability, the as-fabricated snow-TENG has significant potential for wearable electronics, as illustrated in Fig. 6a. When attached to clothing, a snow-TENG can be used not only as a wearable energy harvester for charging electronic devices but also as an active, self-powered multifunctional tracking platform (Fig. 6b and c). Here, the performance of the device depends on the impact force, which in turn

depends on the exact location where it is integrated. For example, the potential difference generated under real snowfall conditions depends on whether the snow-TENG device is attached to the shoulder, wrist or knee area. In these experiments, the electrical outputs from the snow-TENG devices worn on these body parts were obtained in the snowfall mode, where both impact and sliding are responsible for the signal generation. In addition, Fig. 6c shows that a snow-TENG device attached to the sole of a shoe and in direct contact with snow can generate signals that could be used to identify various activities performed by the wearer. The results show that the output signal of the snow-TENG can be used to capture the intensity of motion and its type. This is mainly due to the dependence of the shape of the waveform on the type of activity, as illustrated in Fig. 6c(ii). All the results were measured outdoors, under the following conditions: Temperature of −6 °C, humidity of 60%, wind speed of 15 km/h and snow particle diameters less than 1 cm.

3. Conclusions

In summary, a new all-printable TENG, based on snow triboelectrification, is presented with UV curable silicone as the triboelectric material and PEDOT: PSS as the electrodes, fabricated using a facile 3D printing method. The developed metal-free snow-TENG has been used as an energy harvesting and multifunctional sensing device for snow-related applications. Upon friction/impact with snow, the snow-TENG device in a single electrode mode yields output peak-to-peak V_{oc} and output J_{sc} of up to 8 V and 40 μA/cm^2, respectively. Instantaneous output power density from the snow-TENG achieved 0.2 mW/m^2 when connected to a load resistor of 50 MΩ. Unlike traditional weather stations in cold regions, the snow-TENG has a simple design, low cost, and is maintenance-free. This gives the snow-TENG the ability to be used as a self-powered, sensitive snow-related meteorological monitoring station to measure critical weather parameters, such as snowfall rate, snow depth, wind direction, and speed. In addition, the proposed snow-TENG can be utilized as a sustainable power source for wearable electronics and biomechanical tracking sensors to monitor different human movements, such as running, jumping, walking and marching. This opens the door to a new generation of self-powered wearable e-skin devices for tracking athletes and as an effective detector for avoiding hazards in snow-related sports.

4. Materials and methods

4.1. Materials

Poly (3,4-ethylene dioxythiophene)-poly (styrene sulfonate) 1.1% in H_2O, neutral pH, high-conductivity grade (PEDOT: PSS) and dimethyl sulfate ((DMS, $(CH_3)_2SO_4$), 99.8% purity) were purchased from Sigma Aldrich. Mercapto-functionalized silicones, specifically 13–17% (mercaptopropyl) methylsiloxane-dimethylsiloxane copolymer 1 (SMS-142, 100–200cSt), 2–3% (mercaptopropyl) methylsiloxane-dimethylsiloxane copolymer 2 (SMS-022, 100cSt), α,ω-Vinyl-terminated poly(dimethylsiloxane) copolymers 3 (DMS-V21, MW 3853, viscosity of 100 cSt), 4 (DMS-V31, MW 21500, viscosity of 1000 cSt), 5 (DMS-V35, MW 42300, viscosity of 5000 cSt), and silicone oil or decamethylcyclopentasiloxane (D5, $(Me_2SiO)_5$) were purchased from Gelest. Photoinitiator TPO-L (ethyl (2,4,6-trimethylbenzoyl) phenyl phosphinate) was received as a gift from IGM Resins, Inc.

Preparation of the microstructure pattern—First, a 2 mm thick < 100 > Si wafer was spin-coated with a 40 μm-thick layer of the photoresist. This was followed by photolithographic patterning using a square pattern with a side length of 25 μm [37,38]. KOH solution was utilized to complete the etching process and produce the recessed structures of a square. The patterned silicon wafer was used as a mold and was treated with trimethylchlorosilane (Sigma Aldrich) by gas phase silanization to reduce adhesion to the subsequent layers [21,39]. This functionalized Si mold has been used as a substrate for the extrusion printing of silicone, thus decorating the triboelectric layer with the square patterns. The silicone layer was initially exposed to UV curing with a light intensity of 20 W. After post-curing at a UV intensity of 76 W for 6 min, the micropatterned silicone layer was peeled off from the mold. This silicone layer was used as the tribo-functional layer.

3D Printing of PEDOT: PSS layer—An aqueous dispersion of PEDOT: PSS was used as an ink for the 3D extrusion printing of the electrode layer. The conductive polymer was treated by an inorganic dopant, DMS, in an attempt to enhance the polymer conductivity without compromising its excellent mechanical properties and visible light transparency. The weight ratio of the two components was set at 1:25 to achieve the best conductivity (estimated at 100 S/cm) [40]. This solution was subsequently heated at 100 °C for 2 h to adjust the viscosity of the ink before performing extrusion printing on the stretchable silicone substrate with the squared patterns.

3D Printing of silicone layer—A customized print head system was used for the direct printing of the silicone layer. This system takes advantage of a pneumatic pump (up to 90 psi) with switchable solenoid valves for applying positive pressure to control the flow of the ink through the print head. The speed in x and y directions was adjusted at 500 mm/min, while a commercial extrusion nozzle (25-gauge needle) was connected to the ink reservoir with a blunt tip diameter of 215 μm.

The ink consists of the cross-linkers and receptors indicated in the materials section, combined with TPO-L as a photo-initiator. This silicone layer was printed on top of the PEDOT: PSS and used as the substrate of the snow-TENG. Exposure of this layer to UV light leads to polymer crosslinking and eventually results in a mechanically strong, yet flexible and stretchable, silicone layer. This was achieved using a controllable Omnicure S1000 (Lumen Dynamics) light source that was positioned at a 45° angle to the surface, 4 cm from the extrusion nozzle, producing a light intensity of 2.3 W cm^{-2}. This light source has a broad UV wavelength spectrum in the range of 275–500 nm, and strong intensity of 100 Watts. The printing setup utilized two of these light sources, which has the potential for shortening the cure time and increasing the production efficiency.

Electrical measurements—The output current and voltage were recorded using a voltage preamplifier (Keithley 6514 System Electrometer) that was interfaced with a custom LabVIEW program.

Supplementary Material

Refer to Web version on PubMed Central for supplementary material.

Acknowledgments

A.Ahmed, and I. Hassan contributed equally to this work. This research is partially funded by the Canada Research Chairs Program, Canada First Research Excellence Program through the Global Water Futures Program and the Natural Sciences and Engineering Research Council of Canada of Canada through the Strategic Grant Program. J.F.R., I.M.M., E.E., and G.P. are grateful for financial support from NIH Grant No. ES03154. R.B.K. thanks Dr. Myung Ki Hong Endowed Chair in Materials Innovation at UCLA. M.F.E. would like to extend his sincere thanks to Nanotech Energy, Inc for support. The authors thank Dr. Michael A. Brook and Ms. Sijia Zheng for providing us with the inks. Also, The authors thank Mr. Ayman Negm for discussion on some sections of this work.

References

[1]. Andrews RW, Pollard A, Pearce JM, The effects of snowfall on solar photovoltaic performance, Sol. Energy 92 (2013/06/01/2013) 84–97.

[2]. Dalili N, Edrisy A, Carriveau R, A review of surface engineering issues critical to wind turbine performance, Renew. Sustain. Energy Rev 13 (2) (2009/02/01/2009) 428–438.

[3]. Free M, Sun B, Yoo HL, Comparison between total cloud cover in four reanalysis products and cloud measured by visual observations at US weather stations, J. Clim 29 (6) (2016) 2015–2021.

[4]. Sabatini F, Setting up and managing automatic weather stations for remote sites monitoring: from Niger to Nepal, Renewing Local Planning to Face Climate Change in the Tropics, Springer, 2017, pp. 21–39.

[5]. (2018, 23 October). https://nsidc.org/cryosphere/snow/climate.html.

[6]. Buser O, Aufdermaur A, Electrification by collisions of ice particles on ice or metal targets, Electrical Processes in Atmospheres, Springer, 1976, pp. 294–301.

[7]. Hutchinson W, Ice-crystal contact electrification, Q. J. R. Meteorol. Soc 86 (369) (1960) 406–407.

[8]. Petrenko VF, Colbeck SC, Generation of electric fields by ice and snow friction, J. Appl. Phys 77 (9) (1995) 4518–4521.

[9]. Drake J, Electrification accompanying the melting of ice particles, Q. J. R. Meteorol. Soc 94 (400) (1968) 176–191.

[10]. Gaskell W, Illingworth A, Charge transfer accompanying individual collisions between ice particles and its role in thunderstorm electrification, Q. J. R. Meteorol. Soc 106 (450) (1980) 841–854.

[11]. Latham J, The electrification of snowstorms and sandstorms, Q. J. R. Meteorol. Soc 90 (383) (1964) 91–95.

[12]. Caranti J, Illingworth A, Marsh S, The charging of ice by differences in contact potential, J. Geophys. Res.: Atmosphere 90 (D4) (1985) 6041–6046.

[13]. Jayaratne E, Saunders C, Thunderstorm electrification: the effect of cloud droplets, J. Geophys. Res.: Atmosphere 90 (D7) (1985) 13063–13066.

[14]. Fan F-R, Lin L, Zhu G, Wu W, Zhang R, Wang ZL, Transparent triboelectric nanogenerators and self-powered pressure sensors based on micropatterned plastic films, Nano Lett. 12 (6) (2012) 3109–3114. [PubMed: 22577731]

[15]. Lin ZH, Cheng G, Lin L, Lee S, Wang ZL, Water–solid surface contact electrification and its use for harvesting liquid-wave energy, Angew. Chem 125 (48) (2013) 12777–12781.

[16]. Chen J, et al., Networks of triboelectric nanogenerators for harvesting water wave energy: a potential approach toward blue energy, ACS Nano 9 (3) (2015) 3324–3331. [PubMed: 25719956]

[17]. Ahmed A, et al., Self-powered wireless sensor node enabled by a duck-shaped triboelectric nanogenerator for harvesting water wave energy, Adv. Energy Mater 7 (7) (2017) 1601705.

[18]. Ahmed A, Hassan I, Hedaya M, El-Yazid TA, Zu J, Wang ZL, Farms of triboelectric nanogenerators for harvesting wind energy: a potential approach towards green energy, Nano Energy 36 (2017) 21–29.

[19]. Ahmed A, et al., Environmental life cycle assessment and techno-economic analysis of triboelectric nanogenerators, Energy Environ. Sci 10 (3) (2017) 653–671.

[20]. Ahmed A, et al., Self-adaptive bioinspired hummingbird-wing stimulated triboelectric nanogenerators, Sci. Rep 7 (1) (2017) 17143. [PubMed: 29215064]

[21]. Ahmed A, et al., A washable, stretchable, and self-powered human-machine interfacing Triboelectric nanogenerator for wireless communications and soft robotics pressure sensor arrays, Extreme Mech. Lett 13 (2017) 25–35.

[22]. Ahmed A, Hassan I, Zu J, Design guidelines of stretchable pressure sensors-based triboelectrification, Adv. Eng. Mater (2018) 1700997.

[23]. Yi F, et al., A highly shape-adaptive, stretchable design based on conductive liquid for energy harvesting and self-powered biomechanical monitoring, Science Adv. 2 (6) (2016) e1501624.

[24]. Ahmed A, et al., Fire-retardant, self-extinguishing triboelectric nanogenerators, Nano Energy (2019).

[25]. Ahmed A, et al., An ultra-shapeable, smart sensing platform based on a multimodal ferrofluid-infused surface, Adv. Mater. 0 (0) (2019) 1807201.

[26]. Ahmed A, et al., Design guidelines of triboelectric nanogenerator for water wave energy harvesters, Nanotechnology 28 (18) (2017) 185403. [PubMed: 28397707]

[27]. Zong-Hong L, Gang C, Long L, Sangmin L, Lin WZ, Water–solid surface contact electrification and its use for harvesting liquid-wave energy, Angew. Chem 125 (48) (2013) 12777–12781.

[28]. Liang Q, et al., Highly transparent triboelectric nanogenerator for harvesting water-related energy reinforced by antireflection coating, Sci. Rep 5 (2015) 9080. [PubMed: 25765205]

[29]. Zhang Q, et al., An amphiphobic hydraulic triboelectric nanogenerator for a self-cleaning and self-charging power system, Adv. Funct. Mater 28 (35) (2018) 1803117.

[30]. Marsland F, Lyons K, Anson J, Waddington G, Macintosh C, Chapman D, Identification of cross-country skiing movement patterns using micro-sensors, Sensors 12 (4) (2012) 5047–5066. [PubMed: 22666075]

[31]. Chambers R, Gabbett TJ, Cole MH, Beard A, The use of wearable microsensors to quantify sport-specific movements, Sports Med. 45 (7) (2015) 1065–1081. [PubMed: 25834998]

[32]. Wang ZL, Triboelectric nanogenerators as new energy technology for self-powered systems and as active mechanical and chemical sensors, ACS Nano 7 (11) (2013) 9533–9557. [PubMed: 24079963]

[33]. Fan FR, et al., Highly transparent and flexible triboelectric nanogenerators: performance improvements and fundamental mechanisms, J. Mater. Chem 2 (33) (2014) 13219–13225.

[34]. Kim JH, Yun BK, Jung JH, Park JY, Enhanced triboelectrification of the polydimethylsiloxane surface by ultraviolet irradiation, Appl. Phys. Lett 108 (13) (2016) 133901.

[35]. Kreder MJ, Alvarenga J, Kim P, Aizenberg J, Design of anti-icing surfaces: smooth, textured or slippery? Nat. Rev. Mater 1 (1) (2016) 15003.

[36]. Kwon YH, Shin S-H, Kim Y-H, Jung J-Y, Lee MH, Nah J, Triboelectric contact surface charge modulation and piezoelectric charge inducement using polarized composite thin film for performance enhancement of triboelectric generators, Nano Energy 25 (2016) 225–231.

[37]. Zhu Y, et al., A flexible and biocompatible triboelectric nanogenerator with tunable internal resistance for powering wearable devices, Sci. Rep 6 (2016) 22233. [PubMed: 26916819]

[38]. Wang S, Lin L, Wang ZL, Nanoscale triboelectric-effect-enabled energy conversion for sustainably powering portable electronics, Nano Lett. 12 (12) (2012) 6339–6346. [PubMed: 23130843]

[39]. Dhakar L, Pitchappa P, Tay FEH, Lee C, An intelligent skin based self-powered finger motion sensor integrated with triboelectric nanogenerator, Nano Energy 19 (2016) 532–540.

[40]. Reyes-Reyes M, Cruz-Cruz I, López-Sandoval R, Enhancement of the electrical conductivity in PEDOT:PSS films by the addition of dimethyl sulfate, J. Phys. Chem. C 114 (47) (2010/12/02 2010) 20220–20224.

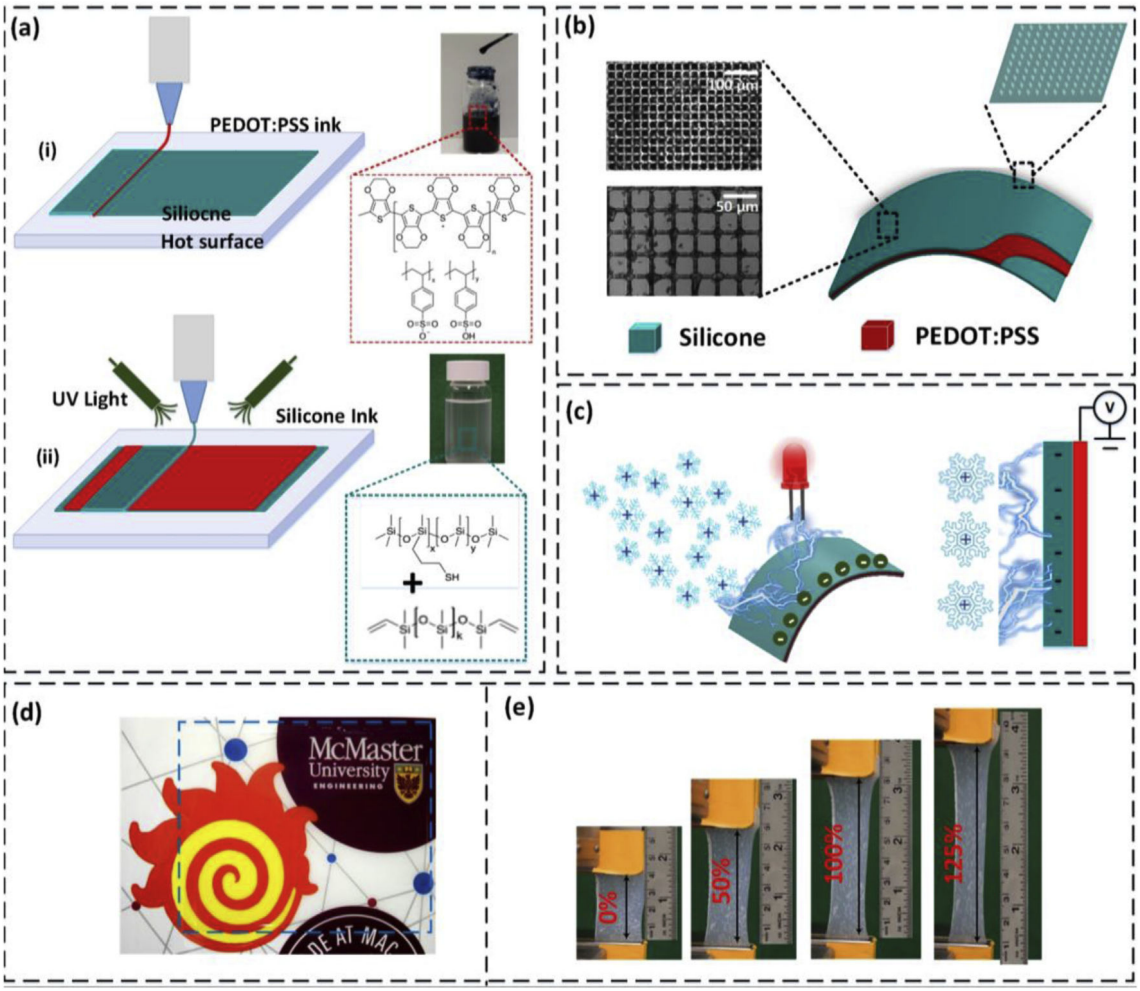

Figure 1. 3D printing process, architecture along with the optical and mechanical properties of a snow-TENG.

(a) Schematic illustration of the printing process of a snow-TENG, **(a–i)** printing of a conductive polymer electrode; inset shows the chemical composition of the PEDOT: PSS ink, **(a-ii)** Printing of the triboelectrification layer based on UV curable silicone ink; inset reveals the chemical composition of the silicone ink. **(b)** Schematic illustration of the structure of the device, featuring a micropatterned surface of the UV curable silicone. SEM images on the left are showing the micropattern at different magnifications. Scale bars are 100 μm and 50 μm, respectively. **(c)** The working principle of the device based on snow triboelectrification. **(d)** A photograph showing the high transparency of the silicone layer; the logo of McMaster University shown in the background can be recognized through the silicone layer. **(e)** Exposure of the snow-TENG to different stretching conditions.

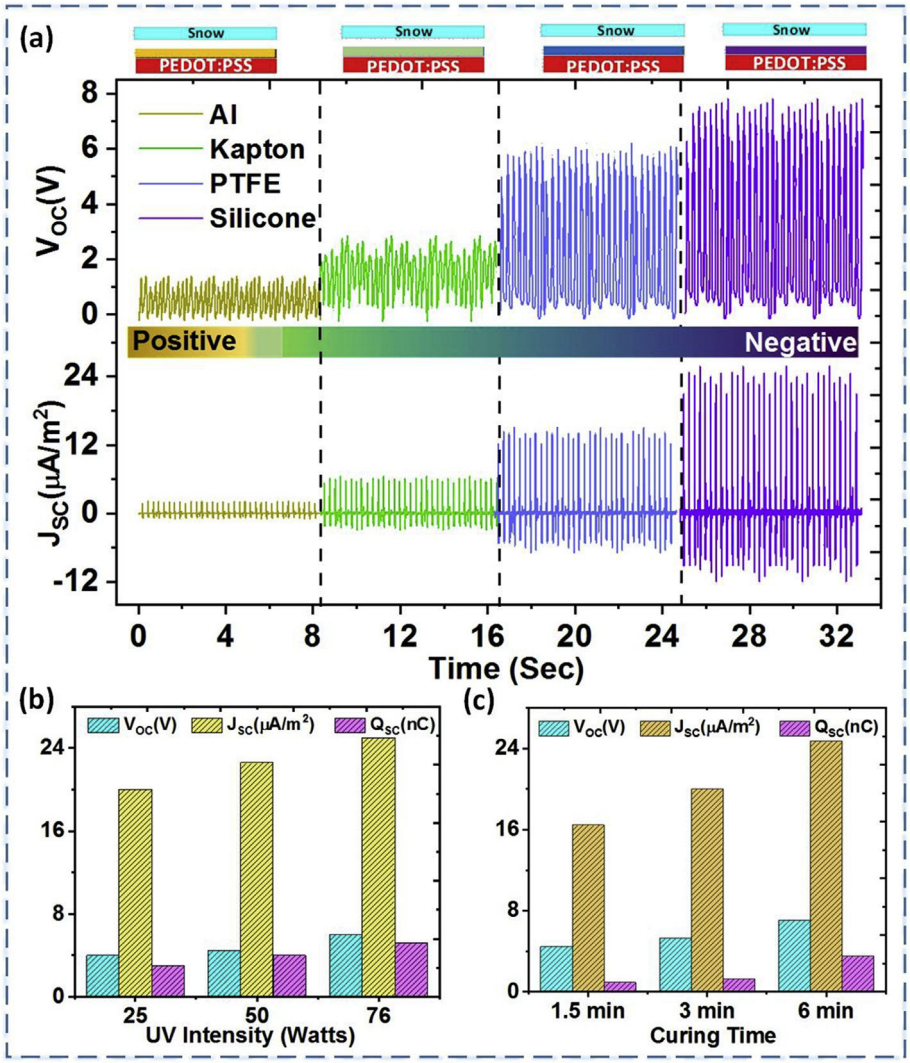

Fig. 2. Evaluation of the electrical performance of a snow-TENG for harvesting energy from falling snow.

(a) V_{OC} and J_{SC} define the triboelectrification performance of a snow-TENG using different positive and negative triboelectric materials. **(b, c)** Influence of the UV light intensity and curing time of the triboelectrification layer (silicone) on the electrical output of the device. The plots compare the open circuit voltage, short-circuit current, and short-circuit charge under different conditions.

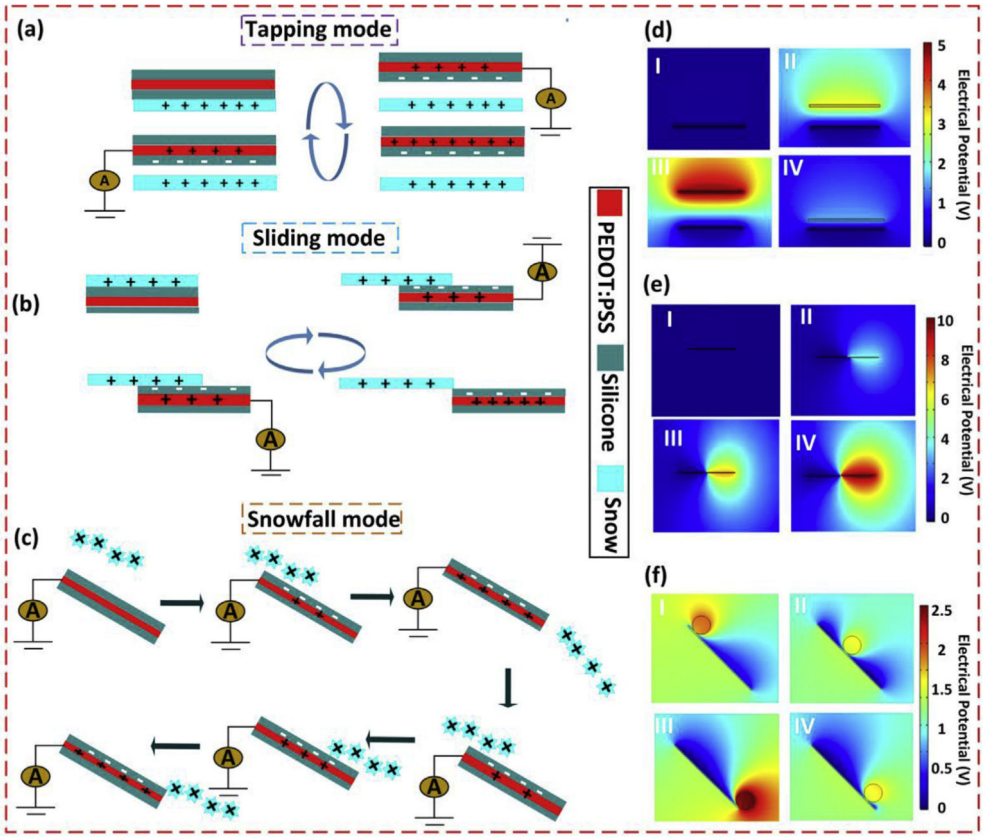

Fig. 3. The working mechanisms and FEM simulations of a snow-TENG.

(a, b, c) Schematic illustration showing the working mechanism of a snow-TENG utilizing three different operating modes including tapping, sliding, and snowfall. **(d, e, f)** FEM simulation results for the corresponding operational modes.

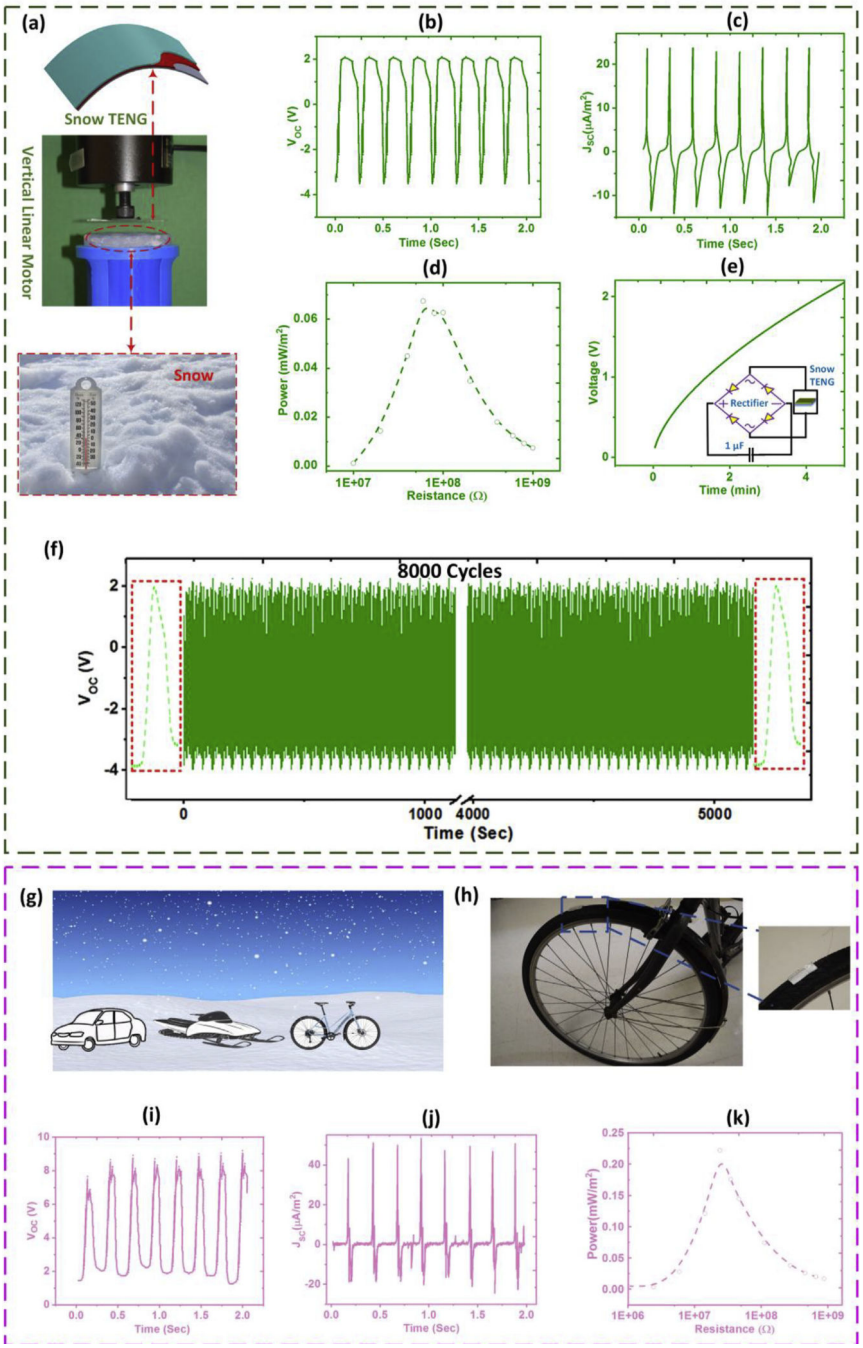

Fig. 4. Characterization of the electrical properties of a snow-TENG in tapping and sliding scenarios.

(a) The testing setup showing a vertical linear motor, snow layer, and the fabricated snow-TENG. **(b)** Open circuit voltage, V_{OC}, **(c)** Short circuit current J_{SC}, and **(d)** External load dependent peak power in the tapping scenario. **(e)** The charging profile of a 1 μF capacitor. **(f)** V_{OC} during 8000 cycles of repeated loading and unloading, reflecting the stability of a snow-TENG device. **(g)** A visionary scene for a snowy location where a snow-TENG can be used for harvesting the energy of moving bicycles or cars. **(h)** A photograph of an energy-

harvesting unit attached to a bicycle. Inset: An actual snow-TENG device on the wheel. **(i)** Measured V_{OC}, **(j)** measured J_{SC}, and **(k)** external load dependent peak power in the sliding scenario.

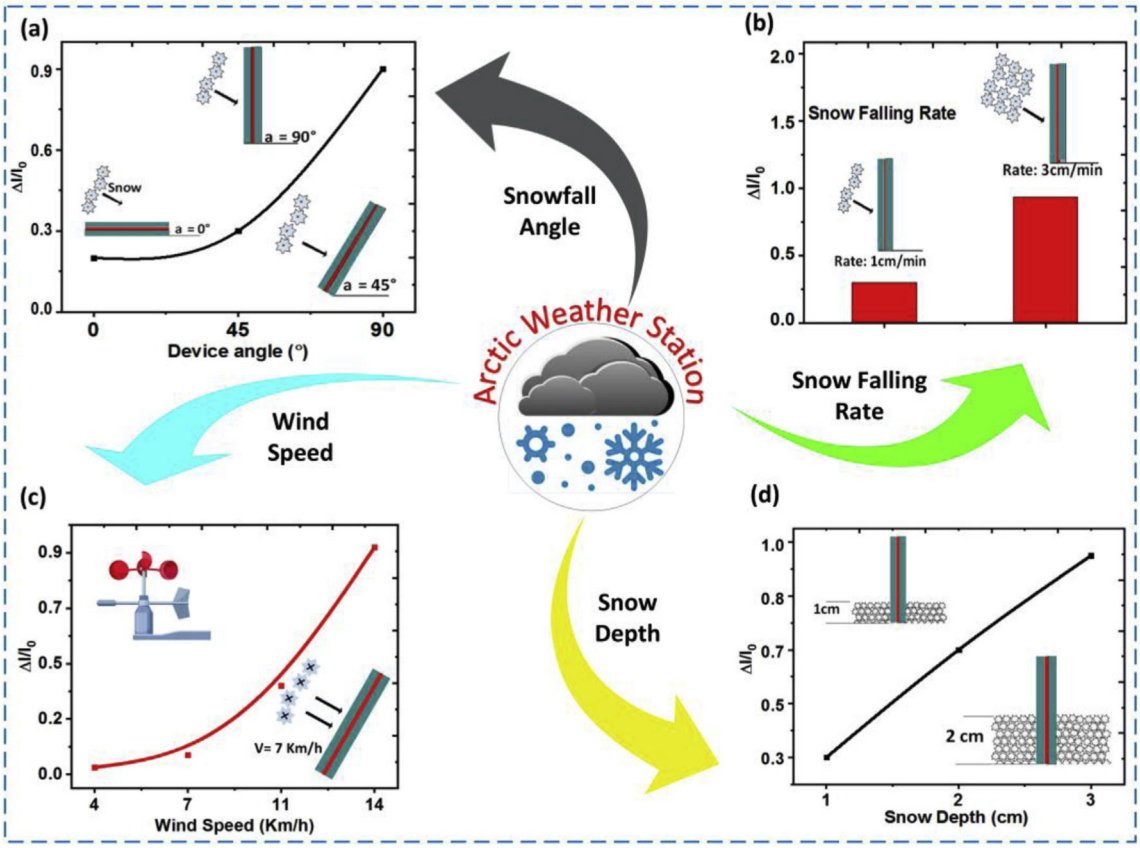

Fig. 5. Snow-TENG as a self-powered arctic weather station.

A snow-TENG can be used as a multifunctional weather station for measuring several functions including **(a)** Snowfall angles or the direction of falling snow. **(b)** Snowfall rate. **(c)** The speed of the wind. **(d)** The snow accumulation depth.

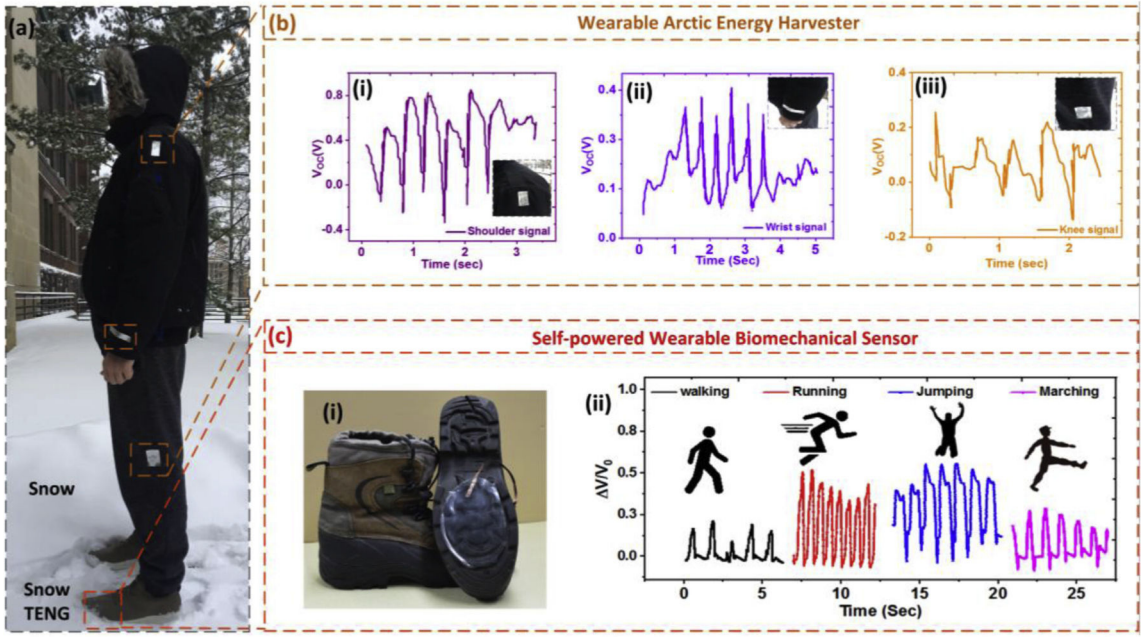

Fig. 6. Investigation of a snow-TENG as a wearable energy harvester and self-powered biomechanical monitor.

(a) Harnessing and sensing biomechanical movements by attaching a snow-TENG to different locations of the human body. **(b)** Measurement of the electrical output from a snow-TENG device that uses a snowfall mode when attached on the **(i)** shoulder, **(ii)** wrist, and **(iii)** knee. **(c–i)** A photograph of the snow-TENG device assembled and attached to the bottom of a snow boot as a self-powered biomechanical sensor. **(c-ii)** Electrical outputs from the snow-TENG as the wearer performs different movements – running, jumping, walking, and marching.